PCCP

Accepted Manuscript

This is an *Accepted Manuscript*, which has been through the Royal Society of Chemistry peer review process and has been accepted for publication.

Accepted Manuscripts are published online shortly after acceptance, before technical editing, formatting and proof reading. Using this free service, authors can make their results available to the community, in citable form, before we publish the edited article. We will replace this *Accepted Manuscript* with the edited and formatted *Advance Article* as soon as it is available.

You can find more information about *Accepted Manuscripts* in the Information for Authors.

Please note that technical editing may introduce minor changes to the text and/or graphics, which may alter content. The journal's standard Terms & Conditions and the Ethical guidelines still apply. In no event shall the Royal Society of Chemistry be held responsible for any errors or omissions in this *Accepted Manuscript* or any consequences arising from the use of any information it contains.

ROYAL SOCIETY OF CHEMISTRY

www.rsc.org/pccp

Journal Name Physical Chemistry Chemical Physics Dynamic Article Links ►

Cite this: DOI: 10.1039/c0xx00000x

www.rsc.org/xxxxxx

ARTICLE TYPE

Spectroscopic and Microscopic Studies of Self-assembled nc-Si/a-SiC Thin Films Grown by Low Pressure High Density Spontaneous Plasma Processing

Debajyoti Das* and Debjit Kar

Received (in XXX, XXX) Xth XXXXXXXXX 20XX, Accepted Xth XXXXXXXXX 20XX
DOI: 10.1039/b000000x

In view of suitable application in the window layer of nc-Si *p-i-n* solar cells in superstrate configuration, the growth of nc-Si/a-SiC composite films were studied, considering the trade-off relation between individual characteristics of it's a-SiC component to provide wide optical-gap and electrically conducting nc-Si component to simultaneously retain enough crystalline linkage to facilitate proper crystallization to *i*-nc-Si absorber-layer during its subsequent growth. Self-assembled nc-Si/a-SiC thin films were spontaneously grown by low-pressure planar inductively coupled plasma CVD, operating in electromagnetic mode, providing high atomic-H density. Spectroscopic simulations of ellipsometry and Raman data, and systematic chemical and structural analysis by XPS, TEM, SEM and AFM were performed. Corresponding to optimized inclusion of C essentially incorporated as Si-C bonds in the network, the optical-gap of a-SiC component widened, void fraction including the incubation layer thickness reduced. While the bulk crystallinity decreased only marginally, Si-ncs diminished in size with narrower distribution and increased number density. With enhanced C-incorporation, formation of C-C bonds in abundance, deteriorate Si continuous bonding network and persuade growth of amorphous dominated silicon-carbon heterostructure containing high-density of tiny Si-ncs. Stimulated nanocrystallization identified in Si-network, induced by limited amount of carbon incorporation, makes the material most suitable for applications in nc-Si solar cells. The novelty of the present work is to enable spontaneous growth of self-assembled superior quality nc-Si/a-SiC thin films and simultaneous spectroscopic simulation-based optimization of properties for utilization in devices.

Introduction

Recently, nano-crystalline silicon (nc-Si) solar cells in the *p-i-n* configuration have emerged as being quite attractive due to the significantly reduced light induced degradation of the *i*-nc-Si layer, compared to its amorphous counterpart, providing better stability to the device.[1, 2] In quest of a suitable window layer for the nc-Si solar cells in superstrate configuration, *p*-type nc-Si/a-SiC composite layer has been identified as the most promising one,[3] as it's a-SiC component could provide a wide optical band gap and the electrically conducting nc-Si component may assist in attaining proper crystallization of the *i*-nc absorber-layer during its subsequent growth.[4-7] However, there is a trade-off relation between the individual characteristics of its two components, similar to other nc-Si dielectric films, e.g., nc-Si/a-SiO and nc-Si/a-SiN.[8-10] Although increasing carbon content in the a-SiC network could provide a wider optical band gap of the window layer, it subsequently produces a poor nc-Si component, leading towards its low electrical conductivity and turning it altogether, as inappropriate for efficient utilization.[11-13] In the present investigation, self-assembled nc-Si/a-SiC thin films are spontaneously grown by low-pressure planar inductively coupled plasma CVD, operating in electromagnetic mode, providing high atomic-H density.[14] Spectroscopic simulations of ellipsometry and Raman data, and systematic chemical and structural analysis by XPS, TEM, SEM and AFM were performed. Corresponding to optimized inclusion of C, when the optical gap widens, Si-ncs diminish in size with narrower distribution and increased number density, maintaining the bulk crystallinity reduced only marginally. Stimulated nanocrystallization in Si-network, induced by limited amount of carbon incorporation, is the prime achievement that makes the material most suitable for applications in nc-Si solar cells. In addition, ensuing analytical techniques and specific spectroscopic simulations could assist in optimization of individual layer thickness, composition and characteristics, and efficiently facilitate utilization of the material in the fabrication of devices.

Physical Chemistry Chemical Physics Accepted Manuscript

Experimental Section

Thin films of nano-crystalline silicon embedded in amorphous hydrogenated silicon carbide (nc-Si/a-SiC) dielectric matrix have been deposited from H_2 diluted (SiH_4 + CH_4) plasma in inductively coupled plasma-aided chemical vapour deposition system (ICP-CVD) excited by radio frequency (rf) of 13.56 MHz. The rf field is generated by means of a four-antenna low inductance flat spiral copper coil which is separated from the vacuum region across a quartz window. In between the quartz plate and the substrate holder, one circular gas ring, a stainless steel grid and another gas ring with smaller diameter are placed sequentially. The grid is kept at electrically floating condition, which actually confines the plasma within the quartz plate and itself, and protects the substrate from direct plasma interaction.[14] The parameters used for the deposition are as follows: substrate temperature at 300°C, rf-Power (13.56 MHz) of 300 W, plasma pressure at 30 mTorr. The SiH_4 and H_2 gas flow were kept fixed at 2 and 38 sccm, respectively, while the CH_4 was introduced systematically so that the flow rate ratio (R) between CH_4 and SiH_4 varied from 0 to 10. The nc-Si/a-SiC films of ~4000Å were deposited on Corning® Eagle 2000™ glass and silicon wafer substrates, whereas specifically for transmission electron microscope studies films of ~400 Å were grown on carbon coated Cu microscope grids, supplied by Pacific Grid-Tech, USA. The spectroscopic ellipsometry measurements were performed at a fixed angle of 70° with Jobin Yvon spectroscopic ellipsometer. Raman spectrum was obtained at room temperature in a backscattering geometry by Renishaw inVia Raman microscope with excitation wavelength of 514 nm from air-cooled Ar+ laser source. The XPS measurements were performed using Omicron X-ray photoelectron spectrometer with a Mg Kα X-ray source. The surface structure of the thin films was characterized by atomic force microscopy (Veeco dI CP II), and a JEOL JSM-6700F scanning electron microscope. The TEM micrographs have been obtained by JEOL JSM 2010 transmission electron microscope operating at 200 kV.

Results

Spectroscopic Ellipsometry

Spectroscopic ellipsometry (SE) is a highly sensitive as well as non-destructive probe to determine the optical properties of solids. It deals with the measurement and interpretation of the changes in the state of polarized light undergoing oblique reflection from a sample surface. The basic observables of the SE are Ψ and Δ, which are the amplitude and phase part of complex reflectance ratio, $\rho = \tan(\Psi)\, e^{i\Delta}$.[15] Signals detected by ellipsometry consist of contributions from different parts of the sample–substrate system. The measured dielectric function, called 'pseudo-dielectric function', <ε>, usually contains information about the whole system, including the substrate, the bulk of the film, the interfaces and surface over layers.[16] The basic concept of ellipsometric data interpretation lies in the comparison of the experimental data to a calculated dielectric function based on a specific model of the sample–substrate system. The contributions of the different parts of the whole system to the pseudo-dielectric function are calculated using Fresnel's equations and combined. The calculated resultant

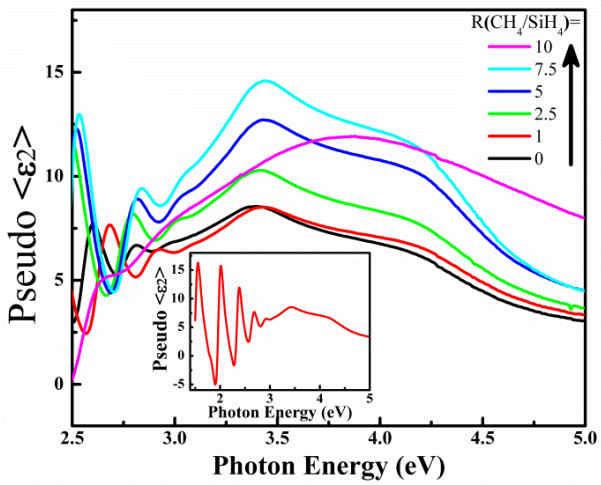

Fig.1 Comparison on the nature of distribution in the imaginary part of pseudo dielectric function, <ε2>, for nc-Si/a-SiC films prepared at varying R (CH_4/SiH_4). Inset shows the typical feature of the < ε2>-spectrum on the entire photon energy range.

dielectric function is then compared to the measured data by performing a least-square-fit to the various parameters of the optical model, e.g., thickness and composition. The classical model calculations are based on the effective medium approximation that describes the dielectric response of a heterogeneous system as a combination of the dielectric functions of its different components.

The inset in Fig. 1 shows the typical distribution of the imaginary part of the pseudo-dielectric function $<\varepsilon_2>$, extracted from the spectroscopic ellipsometry data, for different nc-Si/a-SiC thin films prepared at various flow rate ratios R (CH_4/SiH_4). At low energies, the penetration depth of photons could be larger than the film thickness and that leads to interference fringes due to the interaction between the beams reflected at the film surface and the substrate–film interface. At higher photon energies, the penetration depth decreases until the film is opaque and the reflection at the substrate does not play anymore. So, the oscillations of $<\varepsilon_2>$ at low energies < 3 eV are related to the nature of the substrate, the film thickness and the composition of the first incubation layer, whereas the magnitude of $<\varepsilon_2>$ at high energies is controlled by the bulk composition and the surface roughness.[17]

For the present set of samples, in general for R= 0 and above, the pseudo-dielectric function exhibits two distinct shoulders, around 3.4 and 4.2 eV which can be identified as the critical points (CPs) of the band structure of crystalline silicon, E_1 and E_2, respectively.[18] The appearance of the dual shoulder is the signature of the presence of crystallinity in the film structure. Higher magnitude of $<\varepsilon_2>$ is indicative of higher density of the network.[19, 20] In addition, the intensity difference between these two shoulders corresponds qualitatively to the amount of crystallinity in the network. Continuously increasing magnitude of the $<\varepsilon_2>$ spectra accompanied by two separate shoulders demonstrates the presence of significantly high crystallinity with persistently reduced voids in the nc-Si/a-SiC heterostructure, when prepared with increasing R up to 7.5. However, on farther increase in R= 10, the nature of pseudo-dielectric function changed radically exhibiting a single broad Gaussian-type peak

Physical Chemistry Chemical Physics Accepted Manuscript

This journal is © The Royal Society of Chemistry [year]

centered at 3.88 eV with lower intensity that signifies the formation of amorphous dominated structure of the network. Similar Gaussian-peak for purely a-Si network typically appears at ~3.2 eV. Present shift of the peak towards higher energy could be the consequence of the presence of enough carbon and/or significant fraction of ultra-nanocrystalline Si in the network.[21-23]

The optical properties of the thin films can be obtained from the simulation of the ellipsometry data using proper optical model from those available in the literature, viz., Tauc-Lorentz model (TL), Bruggeman effective medium approximation model (BEMA), Forouhi and Bloomer model (FB) etc.[24,25] The BEMA model has been successfully employed to evaluate the structural composition characteristics of different layer configuration of nano-crystalline silicon thin films grown from H_2-diluted SiH_4 plasma in Hot-wire CVD, Ar-assisted SiH_4 plasma and Ar-assisted H_2-diluted SiH_4 plasma in RF-PECVD.[16,17,26] On the other hand, the TL model has been satisfactorily utilized in determining the size varying changes in the optical properties of Si-ncs embedded in SiO_x matrix, considering the Si:O compositional characteristic of the dielectric matrix remaining unchanged.[22, 23, 27] However, for a thin film system where Si-ncs are embedded in amorphous SiC dielectric matrix, the chemical composition of which changes on sample to sample, it is not practicable to utilize either of the above models alone as none of the individual model can explain such thin film system completely.

In the present investigation, during systematic increase in R (CH_4/SiH_4) in the plasma, C has been increasingly incorporated in the amorphous matrix (without forming crystalline Si-C network [28]) within which embedded Si-ncs change in volume fraction. Hence, the optical property of the amorphous component changes consistently along with the simultaneous changes in the overall structural composition of the network. Accordingly, for proper interpretation on the properties of nc-Si/a-SiC hetero-structure thin films, simulation of the ellipsometry data, for the present set of samples, has been performed using BEMA model in compositional investigation and simultaneously, TL model to account for the changes in the optical properties of the amorphous dielectric matrix, in particular.

In the simulation of the ellipsometry data, a three-layer structure of the film on glass substrate has been considered – (i) a very thin incubation layer with highly amorphous dominated network, immediately on the substrate surface, (ii) bulk layer consisting of a variable composition of nanocrystalline silicon, amorphous silicon carbide and voids and (iii) a thin surface layer (or growth layer) having high void fraction. The BEMA model accompanied by TL model for amorphous part has been applied for each layer. As a reference to TL model the imaginary part of the dielectric function of a-SiC has been considered as developed by Jellison and Modine, in which Tauc joint density of states has

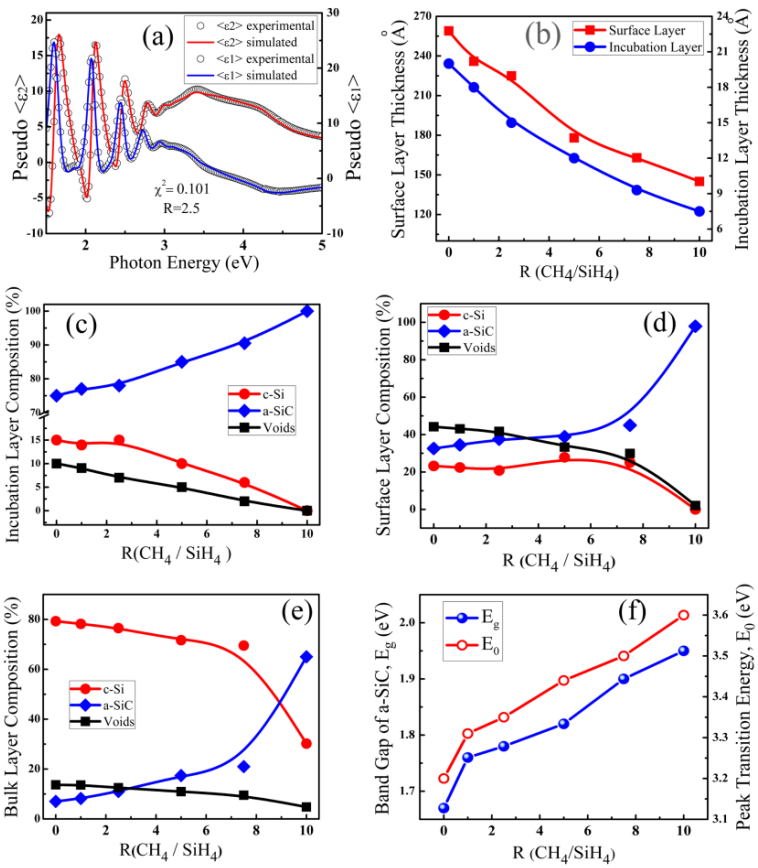

Fig.2 (a) Representative experimental and simulated spectra for the real and imaginary parts of pseudo dielectric function, <ε1> and <ε2> respectively, exhibiting reasonably good match in between. (b) Variations in the individual thickness of the incubation layer and the surface layer of nc-Si/a-SiC films with increase in R. (c-e) Variations in the composition of each individual layer as function of increasing R, demonstrating a gradual change in the network from nano-crystalline to amorphous dominated structure. (f) Widening of the band gap and peak transition energy of the a-SiC component of each film, as estimated using TL model, on varying R.

Physical Chemistry Chemical Physics Accepted Manuscript

been taken into account with Lorentz oscillator. The TL formalism can be written as the following equation:

$$\varepsilon_2 = \frac{1}{E}\frac{A*E_0*B*(E-E_g)^2}{(E^2-E_0^2)^2+B^2*E^2} \quad \text{for } E > E_g$$

$$= 0 \quad \text{for } E \le E_g \qquad (1)$$

where, E_0, E_g, B and A are the peak transition energy, optical gap, broadening factor and amplitude (corresponding to oscillator strength) respectively.[24,29,30] The real part of dielectric function can be calculated using Kramers-Kronig integration formula as shown below.

$$\varepsilon_1 = \varepsilon_1(\infty) + \frac{2}{\pi} P \int_{E_g}^{\infty} \frac{\xi\varepsilon_2(\xi)}{\xi^2 - E^2} d\xi \qquad (2)$$

where, P is the principal part of the Cauchy integral and $\varepsilon_1(\infty)$ stands for the magnitude of ε_1 at the infinity. In the present simulation, both the imaginary and real part of dielectric function has been fitted. The goodness-of-fit has been estimated by the χ^2 value, calculated by Marquardt formula.[31] The magnitude of χ^2 for simulations for each film was below 0.2, implying high degree of goodness-of-fitting. Fig. 2(a) demonstrates a visual justification of the fitting between the experimental and simulated spectra for both the real and imaginary part of dielectric function for R=2.5.

Fig. 2 (b-e) show the variation of thickness and composition of each individual layer as a function of increasing R, obtained from the simulation of the ellipsometry data. The incubation layer is basically amorphous dominated that includes only ~15% crystallinity and ~ 10% void within its thickness of ~ 20 Å at R=0. Both crystalline and void fractions gradually reduce along with the continuous reduction in layer thickness with increasing R, and a purely amorphous incubation layer of ~ 7.5 Å is obtained at R=10 (Fig. 2b & 2c). Relatively high void density (>40%) of the surface layer along with its thickness (>250 Å) gradually reduce with increasing R (Fig. 2b & 2d). The overall crystallinity in the bulk of the material reduces almost linearly from ~80% at R=0 to ~70% at R=7.5, beyond which the nature of the material sharply changes towards an amorphous dominated structure. At R=10, mostly a-SiC film containing ~30% nc-Si is obtained, as shown in Fig. 2(e). The void density in the bulk layer reduces spontaneously from ~14% at R=0 to ~5% at R=10.

The optical gap energy (E_g) of the dielectric a-SiC matrix component and the peak transition energy (E_0) have been

Table 1 The variations in the parameters of Tauc-Lorentz model of a-SiC for thin films prepared at different R.

$R(CH_4/SiH_4)$	Oscillator Amplitude (A)	Broadening Parameter (B)	Offset (ε_∞)
0	131.4	1.54	0.50
1	117.2	1.33	0.57
2.5	155.4	1.61	0.81
5	125.2	1.69	1.48
7.5	143.5	1.52	0.9
10	152.2	2.99	1.21

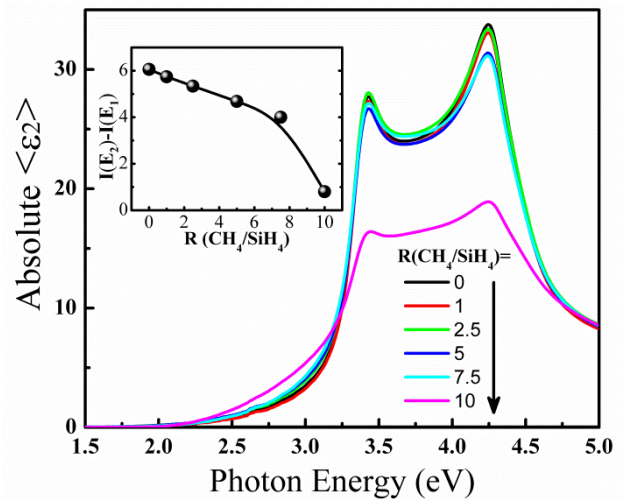

Fig. 1 The spectra of imaginary part of the absolute dielectric function of the bulk material at different R, as estimated from SE data simulation. Inset shows the lowering of difference between the intensities of two critical points (E_2 and E_1) of crystalline silicon at increasing R, possibly implying decaying crystallinity.

estimated from ellipsometric simulation using the TL model. Fig. 2(f) shows that E_g increases from 1.67 eV at R=0 to 1.95 eV for R=10, while E_0 increases from 3.2 eV to 3.6 eV. The increase in both E_g and E_0 can be attributed to the probable enhancement of the density of Si-H and Si-C bonds with increasing R. The other parameters of TL model have been listed in Table 1. The broadening parameter, B, does not vary significantly for $0 \le R \le 7.5$, but at R=10 it suddenly rises to a magnitude of 2.99. The invariance of the broadening factor indicates the merely changed crystalline nature of the films for $0 \le R \le 7.5$, whereas abrupt increase in the broadening factor signify a rapidly increasing structural disorder in the Si–C–H heterostructure and a subsequent sudden decay in crystallinity due to considerably fast incorporation of C during $7.5 < R \le 10$.[21]

The estimated structural composition for the bulk layer has been utilized to generate the absolute dielectric function of the bulk films, excluding any contribution from substrate or surface layer. Fig. 3 represents the imaginary part $<\varepsilon_2>$ of the absolute dielectric function for the nc-Si/a-SiC films prepared at different R. The intensity difference ($I_{E2} - I_{E1}$) between two critical points (E1 and E2) at 3.43 eV and 4.24 eV, plotted against R, as shown in the inset of Fig. 3, indicates a nature of variation of crystallinity of the films which closely resembles with the similar variation of estimated crystallinity in the bulk, especially a sharp transition at $7.5 < R \le 1$, as plotted in Fig. 2(e).[17]

Raman Spectroscopy

After exploring the compositional characteristics of the nc-Si/a-SiC heterostructure and the optical properties of the dielectric a-SiC matrix through ellipsometric simulation, let us now try to probe on the nature of variations in the average size as well as the size-distribution of the silicon nano-crystals and their percentage composition in the bulk, using Raman analysis. Raman spectroscopy is a very powerful non-contact tool to analyze the crystalline properties of silicon in an amorphous matrix. Fig. 4(a)

Physical Chemistry Chemical Physics Accepted Manuscript

This journal is © The Royal Society of Chemistry [year]

Cite this: DOI: 10.1039/c0xx00000x

www.rsc.org/xxxxxx

ARTICLE TYPE

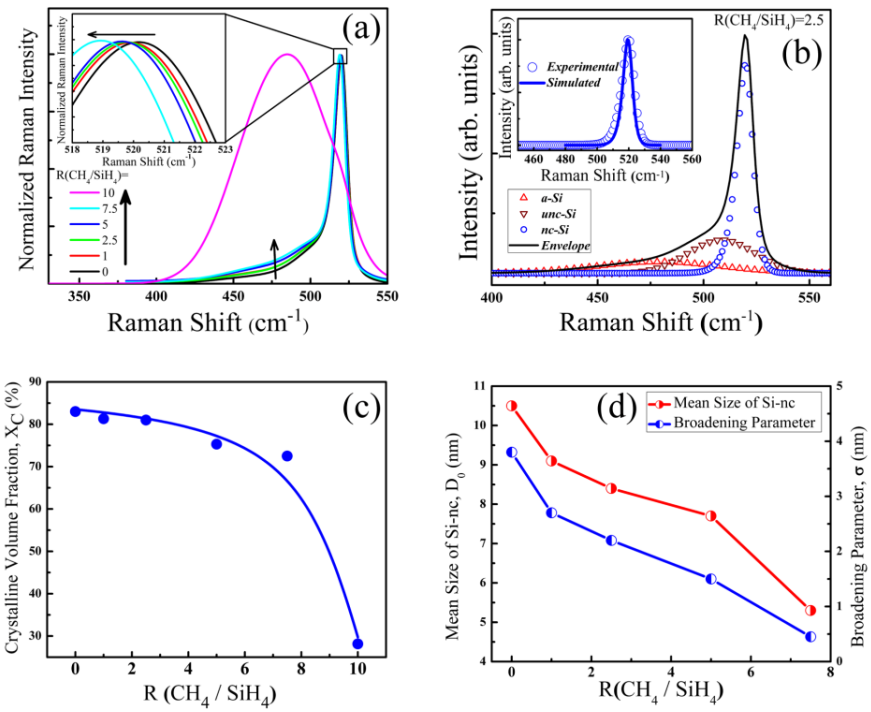

Fig. 2 (a) Normalized Raman spectra of nc-Si/a-SiC thin films prepared at different flow rate ratio (R). The gradual shifting of peak position is observable from the magnified view in the inset. (b) A typical de-convoluted Raman spectrum for nc-Si/a-SiC film. Inset shows the goodness-of-fitting of nc-Si peak, between the experimental data and the simulated data from phonon confinement model with the consideration of Gaussian size-distribution of Si-nc. (c-d) The decaying crystallinity (as estimated from Raman spectroscopy), and the variations of the mean size of Si-nc and the corresponding broadening (or size-distribution) parameter as estimated from the phonon confinement model, at varying R.

shows the normalized Raman spectra for the films prepared at different R. It is noted that for $0 \leq R \leq 7.5$, the Raman spectra closely resembles with each other having very sharp features at higher wave number with shallow extension at lower wave numbers. However, careful observation at the inset reveals that the sharp peak undergoes a systematic red-shift, while the broad extension at lower wave number monotonically increases in intensity at increasing R that turns to a large Gaussian peak around 480 cm^{-1} for R= 10. Each spectrum was deconvoluted into three satellite components consisting of a sharp distribution at ~520 cm^{-1}, a broad distribution at ~480 cm^{-1} and an intermediate component in between 500-510 cm^{-1},[32] as shown in Fig. 4(b). The detailed information of the de-convoluted spectra for each film has been presented in the Table 2. In the deconvoluted spectra the sharp peak is due to nano-crystalline silicon (nc-Si) and the broad peak is assigned for amorphous silicon (a-Si), whereas the intermediate component has been associated to the ultra-nano-crystalline silicon (unc-Si) [33,34] or dilated Si-Si bond near grain-boundary regions.[35] The crystalline volume fraction X_C for films prepared at different R is determined from the de-convoluted peaks using the following formula

$$X_C = \frac{(I_{nc} + I_{unc/gb})}{(I_{nc} + I_{unc/gb} + \beta I_a)} \quad (3)$$

where, I_{nc}, $I_{unc/gb}$ and I_a are the integrated intensities for the peaks corresponding to nano-crystalline, ultra nano-crystalline (or grain boundary) and amorphous components of the deconvoluted peaks. Here β represents the ratio of cross sections of crystalline silicon to amorphous silicon and for nano-crystalline silicon thin film β can be taken as unity.[36] A gradual reduction in X_C within a limited range from ~83 to 73% was estimated for increasing R from 0 to 7.5, beyond which X_C reduced sharply to ~28% at R= 10, as shown in Fig. 4(c). It is markedly noted that the nature of variation as well as the magnitude of crystallinity of the films estimated from Raman studies match excellently with that for the bulk of the material obtained from ellipsometric modelling. In view of the gradual shift, towards lower wavenumber, of the individual peak position of the satellite component of the Raman peak corresponding to nc-Si segment, as demonstrated in Table 2, Raman data were simulated considering the phonon confinement effect arising due to miniaturization of Si-ncs with Gaussian size distribution. To describe the phonon confinement effect, a sine wave has been taken as the confinement function which vanishes

Physical Chemistry Chemical Physics Accepted Manuscript

Cite this: DOI: 10.1039/c0xx00000x

www.rsc.org/xxxxxx

ARTICLE TYPE

Table 2 The Raman data of the de-convoluted peaks for different nc-Si/a-SiC thin films prepared at different R.

R (CH_4/SiH_4)	nc-Si peak		unc-Si peak		a-Si peak	
	Position (cm^{-1})	FWHM (cm^{-1})	Position (cm^{-1})	FWHM (cm^{-1})	Position (cm^{-1})	FWHM (cm^{-1})
0	519.6	9.17	507.59	36.36	478.03	73.2
1	519.42	9.01	507.72	37.0	478.04	69.4
2.5	519.38	8.97	507.98	37.25	478.07	68.41
5	519.24	8.55	508.52	36.75	479.67	67.24
7.5	518.55	8.46	507.11	38.08	476.9	68.33

outside the nc-Si boundary and the phonon dispersion curve has been takes as proposed by Paillard.[37] The final expression for the first order Raman spectrum is

$$I(\omega, D) \approx \int_0^{0.5} \frac{Sin^2[(qD/a)\pi]dq}{[1-(qD/a)^2]^2[\varpi(q)-\omega]^2+(\Gamma/2)^2]} \quad (4)$$

where, a is the lattice parameter (0.543 nm), Γ is the natural line-width of bulk c-Si peak which has been taken as 6 cm^{-1} considering the instrumental broadening factor into account. The $\varpi(q)$ is the phonon dispersion relation given by

$$\varpi(q) = \sqrt{(520)^2 - \frac{121600 \times q^2}{q+0.53}} \quad (5)$$

The above Equations (4) and (5) are appropriate for silicon nano-crystals with uniform size, i.e. where the grain size D does not have any distribution. However, in reality the Si-ncs must have a separate size distribution in each sample. Accordingly, the final expression for the Raman spectrum can be written as[38, 39]

$$I(\omega) \propto \int f(D) I(\omega, D) dD \quad (6)$$

where, $f(D)$ has been taken in the Gaussian size-distribution as

$$f(D) = \left(1/\sigma\sqrt{2\pi}\right) \exp\left(-\frac{(D-D_0)^2}{2\sigma^2}\right) \quad (7)$$

Here, D_0 is average grain size of nc-Si (apex of the Gaussian distribution) and σ is the size distribution parameter.[40] The components of the Raman spectra corresponding to the nc-Si segment, with peak positions 520 > ω (cm^{-1}) > 518, were simulated based on above formulation and excellent agreement with deconvoluted experimental data for nc-Si component was attained for 0 < R < 7.5. A typical simulation data has been shown at the inset of Fig. 4(b) for the film prepared at R=2.5. The experimental data cannot be matched well with the simulated one for R= 10, where the network grossly deviates from crystallinity.

The average grain size (D_0) of the nc-Si and the corresponding size-distribution parameter (σ), called the 'broadening parameter', as estimated from the above simulation of the Raman data for the films prepared at varying R, have been plotted in Fig. 4(d). The average grain size was estimated to reduce from 10.5 nm to 5.3 nm whereas the size-distribution parameter systematically decreased from 3.8 nm to 0.45 nm. Accordingly, a spontaneous miniaturization of Si-ncs with simultaneous narrowing in size distribution has been obtained in the Si-C-H heterostructure on increasing R in the plasma, as demonstrated by the present simulation of the Raman data.

X-ray Photoelectron Spectroscopy

The elemental compositions of Si and C and their various inter bonding ratios in the nc-Si/a-SiC hetero-structure thin films have been studied by X-ray photoelectron spectroscopy (XPS). Fig. 5 shows a wide scan XPS-spectrum for R=10. The prominent peaks of the spectrum are at ~ 100 eV, 150 eV and 285 eV, which correspond to Si 2p, Si 2s and C 1s, respectively.[41] Each elemental

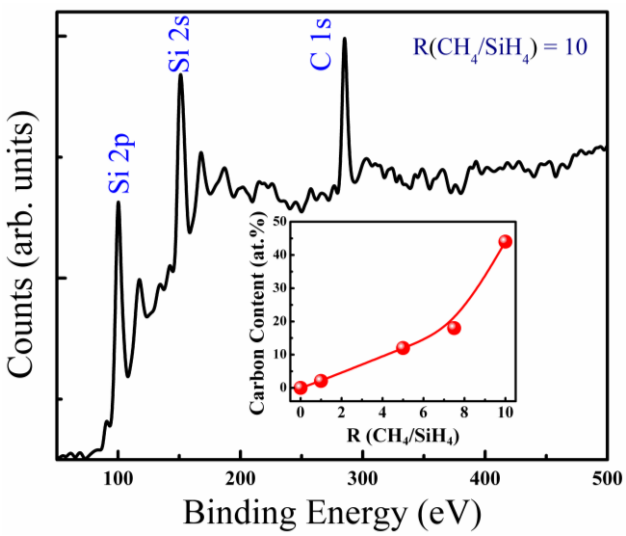

Fig. 3 A typical wide-scan spectrum of X-ray photoelectron spectroscopy (XPS) for nc-Si/a-SiC film prepared at R=10, showing peaks corresponding to Si 2p, Si 2s and C 1s. Inset shows the enhancement of the atomic concentration of carbon due to increase in R, with a sharp rise for R>7.5.

Physical Chemistry Chemical Physics Accepted Manuscript

composition can be estimated from the following formula:

$$X\,(at.\%) = 100\% \times \left(\frac{I_X}{S_X}\right) \Big/ \sum_{i=1}^{N}\left(\frac{I_i}{S_i}\right) \qquad (8)$$

where, I_X and S_X are the integrated intensity and sensitivity factor for the element X. The sensitivity factors for Si 2p and C 1s have been taken as 0.37 and 0.31, respectively.[42] The nature of variation of increasing C-content (with proportional error varying from 0.03–0.05%) in the films with increasing R in the plasma has been shown at the inset in Fig. 5. The carbon content in the nc-Si/a-SiC hetero-structure increases almost linearly, attaining ~18 at.% for R=7.5 beyond which a very rapid incorporation of C in the network has been identified. The material contains ~44 at.% of C for R=10 which is still <50% that implies formation of silicon-rich silicon carbide thin films.

To get elaborate information about the nature of bonding between Si and C in the deposited films, high resolution (HR) scan XPS has been performed for Si 2p and C 1s peaks. The HR scan spectra for Si 2p show asymmetric peaks centered at 99.3 eV with the elongated tails towards higher binding energy, as shown in Fig. 6 (a). The de-convoluted spectra exhibit the presence of two distinct Gaussian peaks centered at ~ 99.1 eV and 99.6 eV, which are assigned to Si-Si bond and Si-C bond respectively.[43] Similar deconvolution to the HR scan spectra of C 1s (Fig. 6(b)) representing asymmetric peaks centered at 285.2 eV, identifies two satellite Gaussian components at ~ 285 eV and 286.6 eV which are attributed to the C-Si and C-C bonds, respectively.[44] The individual integrated areas under Si-C ($I_{Si\text{-}C}$) and Si-Si ($I_{Si\text{-}Si}$) as well as under C-C ($I_{C\text{-}C}$) and C-Si ($I_{C\text{-}Si}$) were estimated for each sample. Fig. 6(c) represents the variations of the ratios ($I_{Si\text{-}C}/I_{Si\text{-}Si}$) and ($I_{C\text{-}C}/I_{C\text{-}Si}$) as a function of increasing R. It is noted that after the initial incorporation of C in the Si-network at R=1, the Si-C bond density increases linearly within the Si-Si matrix for 1<R<7.5 during which the C-C to C-Si bond density ratio remains virtually unchanged. However, for R>7.5 the Si-C bond density increases very rapidly along with a subsequent sharp increase in C-C to C-Si bond ratio. Accordingly, it signifies a notable transition in the process of C incorporation in the Si-network wherein a rapid C-intake occurs (Fig. 6(c)) mostly in the form of C-C bonding, thereby terminating the growth of perpetual Si-network and persuading an amorphous as well as C dominated structure (Fig. 4(c)), for increasing CH_4-to-SiH_4 ratio in the plasma, at R>7.5.

Bulk microstructure by TEM

Systematic changes in the evolution of silicon nano-crystals (Si-ncs) within the surrounding a-Si matrix having continuously increasing carbon content, have been investigated by transmission electron microscopy. Silicon nano-crystals are, in general, observable in the micrographs as dark spots randomly distributed in a relatively bright amorphous matrix. The statistical analysis of the size distribution of Si-nc embedded within the a-SiC matrix are typically presented by the histograms shown in the insets of Fig. 7(a-b). The corresponding high resolution images demonstrate lattice planes of silicon crystals with both <111> and <220> crystallographic orientations, with sharp edge separating

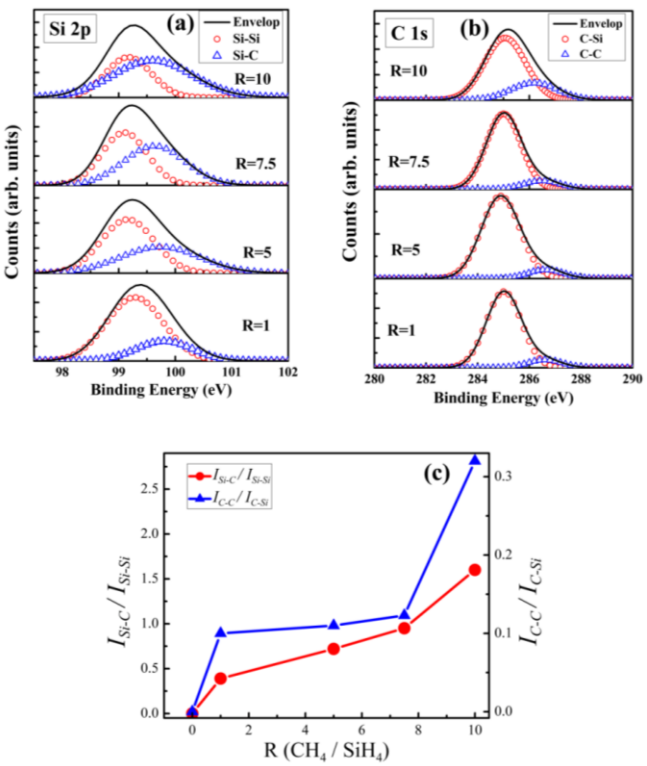

Fig. 4 (a) The deconvoluted high resolution scan spectra for Si 2p at different R, demonstrating gradual changes in the relative strength of Si-Si and Si-C components. (b) The deconvoluted high resolution scan spectra for C 1s for thin films prepared at various R, demonstrating gradual changes in the relative strength of C-Si and C-C components. (c) The individual nature of increasing contributions of the $I_{Si\text{-}C}/I_{Si\text{-}Si}$ and $I_{C\text{-}C}/I_{C\text{-}Si}$ fractions estimated from the deconvoluted spectra of Si 2p and C 1s, with increasing R in the plasma.

Physical Chemistry Chemical Physics Accepted Manuscript

Cite this: DOI: 10.1039/c0xx00000x

www.rsc.org/xxxxxx

ARTICLE TYPE

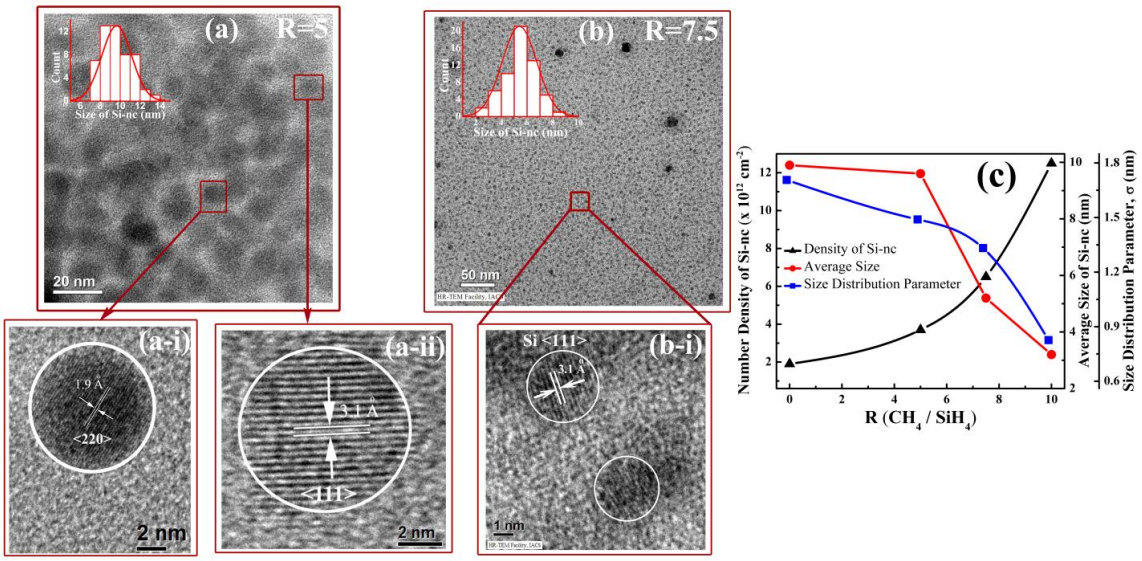

Fig. 7 (a-b) TEM micrographs of the nc-Si/a-SiC heterostructure prepared at R = 5 and 7.5. The histograms at the inset show the size distribution of nc-Si grains for each film. (a-i), (a-ii) and (b-i) present the corresponding high resolution TEM images, demonstrating the lattice planes of c-Si with <111> and <220> crystallographic orientations. (c) The variation of the average grain size, size-distribution parameter (or broadening parameter) and the average number density of Si-ncs, as calculated from the TEM histograms at different R.

the crystallites from the amorphous region. Along with gross reduction in the overall crystallinity, high magnitude of R results in a drastic diminution of the size of Si-nc, as plotted in Fig. 7(c). The average grain size (the apex of the Gaussian distribution) reduced from ~10 nm to ~3 nm whereas the size-distribution (broadening) parameter decreased from 1.7 nm to 0.8 nm, along with simultaneous increase in number density of Si-ncs from 1.9 x 10^{12} cm^{-2} to 1.2 x 10^{13} cm^{-2}, as consequence of increasing carbon incorporation.[10]

Surface analysis by SEM and AFM

The morphological characteristics of film surface have been investigated by scanning electron microscopy (SEM), along with its three dimensional topography using atomic force microscopy (AFM). Fig. 8(a-i) and (b-i) represent the SEM pictures of the surface for the films prepared at R=0 and 10, while the corresponding AFM topography are demonstrated by Fig. 8(a-ii) and (b-ii), respectively. The film prepared at R=0 shows large clusters on the surface which are irregular in size, closely packed with each other, however, maintain notable concentration of voids which are attributed to the superior crystallinity in the film network. Increase in R results in improved film surfaces in terms of smaller cluster size and reduced voids in between them, providing a relatively compact network structure. The systematic reduction of the RMS roughness of the surface with increasing R (Fig. 8(c)), as estimated from 3D images, closely resembles with the lower void fraction in the surface layer of the corresponding lesser crystalline film, as obtained from the ellipsometric simulation.

Discussions

The spectroscopic ellipsometry data for nc-Si/a-SiC hetero-structure thin films have been simulated using BEMA model in compositional investigation and simultaneously by TL model to account for the changes in the optical properties of the amorphous dielectric matrix, in particular. From the systematic studies on different individual layers, it has been identified that the mostly amorphous incubation layer of the even non-carbonated film (nc-Si/a-Si) prepared at R=0 possess a very low incubation layer thickness ~20 Å. In case of similar films prepared by regular capacitively coupled rf glow discharge CVD, normally the incubation layers are much thicker and purely amorphous.[16,45] Formation of relatively thin incubation layer possessing even ~15% crystallinity for the present sample is the courtesy of inductively coupled plasma CVD, operating in the electromagnetic mode, that facilitates the growth by providing high density of atomic hydrogen in the plasma [46,47] produced by its inherent high electron density n_0 ~ 10^{12} cm^{-3} even at low pressure of tens of mTorr.[14,48] For the nc-Si/a-SiC films prepared at increasing R in the range $1 \leq R \leq 10$, the incubation layer further reduces in thickness down to ~ 7.5 Å, although the crystallinity gradually diminishes. Particularly for the development of nc-Si solar cells, a typical requirement of *p*-nc-Si/a-SiC layer is ~200 Å where in the confinement of the incubation layer within about 10 Å will be significant such that the subsequent bulk component could provide effective crystalline/conducting interconnection.[5,7,11,49,50] Regarding the bulk layer composition, a

Physical Chemistry Chemical Physics Accepted Manuscript

Cite this: DOI: 10.1039/c0xx00000x

www.rsc.org/xxxxxx

ARTICLE TYPE

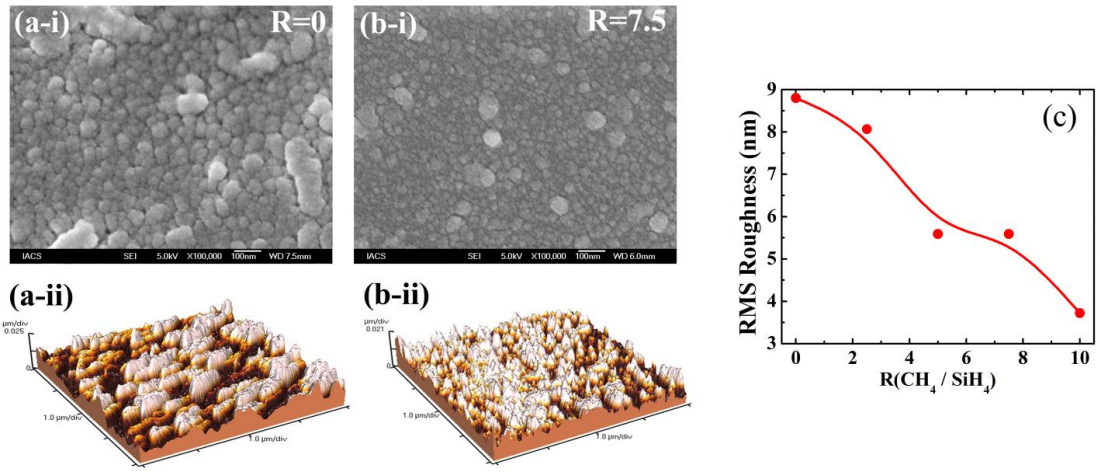

Fig. 8 (a-i) and (b-i) FESEM images of nc-Si/a-SiC films prepared at R=0 and 7.5. (a-ii) and (b-ii) 3D surface morphology by AFM, for the nc-Si/a-SiC films prepared at R=0 and 7.5. (c) Reduction of surface roughness estimated from the AFM data, with the increase in R in the plasma.

high magnitude of crystallinity ~80-70% is maintained for increasing R up to 7.5 at which the void fraction reduces down to ~10%. While preparing solar cells with a µc-Si *i*-layer, a *n*-µc-SiC window layer prepared by Hot Wire CVD has been reported to obstruct the spontaneous sequential growth of a high quality *i*-µc-Si layer on it, without using a seed layer in between.[51] This was because of obvious lattice mismatch between *n*-µc-SiC and *i*-µc-Si that introduced a reasonably thick incubation layer at the interface. While the presently developed nc-Si/a-SiC material, with its wide optical band gap and reasonably high nc-Si volume fraction (~70%) having extremely low self incubation thickness (~9 Å), possess enough prospect for its future use in the window layer of solar cells with the µc/nc-Si *i*-layer, in particular.

Corresponding enhancement in the optical gap of the a-SiC component extends from 1.67 to 1.90 eV, making the material favourable for using in the window layer of solar cells. The inclusion of CH_4 in the (SiH_4 + H_2) plasma acts as a dual source for carbon and hydrogen and the increasing R enhances both the Si-C and Si-H bond concentrations in the network. The widening of the optical gap might be due to lowering of valence band edge as a consequence of replacement of weaker Si-Si bonds by stronger Si-C bonds.[52] Moreover, increasing hydrogenation at higher R in the plasma might result in recession in the Si valence band which could help in broadening the optical gap.[53]

The crystallinity of the bulk layer estimated from ellipsometric simulation nicely matches with that of the entire film obtained from the Raman analysis, both in terms of magnitude as well as in its nature of variation with increasing R. The simulation estimated void density at the surface over-layer gradually reduces with increasing R, corroborating the similar trend obtained from visual realization of surface smoothness by scanning electron as well as atomic force microscopy and the associated evaluation of RMS surface roughness. In addition to identifying a systematic reduction in crystallinity, Raman analysis demonstrated a gradual reduction in the size of Si-nanocrystals along with the lowering of the broadening parameter. Excellent verification on the nature of size reduction of the isolated Si nanocrystals embedded in the a-SiC matrix from ~10 to 3 nm including its narrower size distribution, has been obtained from the transmission electron microscopy images and related evaluation. The number density of the Si-ncs simultaneously increased from 1.9 x 10^{12} cm^{-2} to 1.2 x 10^{13} cm^{-2}. Accordingly, stimulated nano-crystallization has been identified to efficiently occur in the Si network induced by limited amount of carbon incorporation and consequently, the material appears suitable for applications in nc-Si solar cells, in particular. Ensuing induced nanocrystallization to the silicon-carbon heterogeneous structure has been effective within inductively coupled plasma due to its relatively high electron density and low electron temperature compared to conventional capacitively coupled plasma and, in particular, by virtue of its unique remote plasma characteristics and low plasma sheath potentials (several or tens of volts) near the deposition substrate which grossly reduce the ion bombardment on the deposited films.[14]

The growth of nanocrystalline silicon thin films by plasma processing is mostly influenced by the presence of high atomic-H density in H_2-diluted SiH_4 at high level of electrical excitation. The growth of silicon thin-films, from SiH_n radicals in the plasma, begins with an incubation layer on the substrate surface and that happens to be mostly defective and amorphous in nature, even in crystalline prone parametric conditions, because of the inherent lattice mismatch between the substrate material and the interacting Si precursors. Voids are formed within the incubation layer in order to minimize strain in the network. Crystallization slowly starts within the incubation layer which gradually turns into the bulk network possessing enhanced crystallinity, during continued growth. The growing surface of the film which remains in contact with the reactive plasma is again defective and

Physical Chemistry Chemical Physics Accepted Manuscript

sufficiently populated with voids. The growth-zone at the sub-surface region plays a vital role in forming the bulk of the network from the plasma contributions. The crystallization process is controlled sensitively by the intensity of atomic-H density near the growing film surface. There are various intriguing processes involved in the crystallization at the growth zone, e.g., abstraction of hydrogen bonded to Si, breaking of weak Si–Si bonds, recombination of precursors through chemical transport, formation of Si–H bonds by re-hydrogenation of surface dangling bonds, diffusion of atomic H into the Si-matrix and chemical etching through formation of SiH_n radicals.[54] These reactions are competitive on the surface induced by atomic H of the plasma and result in the final film structure guided by the parametric conditions. The inherent high atomic-H density of the ICP-CVD systems can provide efficient nano-crystallization to the incubation layer, leaving effectively reduced amorphous counterpart and grossly eliminated void fraction, thereby thinning the incubation layer significantly. The crystallization of the bulk layer can then be adequately boosted up due to the presence of plenty of nano-crystallites in the incubation layer. Furthermore, in a silicon-hydrogen-carbon heterostructure system, increasing carbon content in the primary silicon network, in general, introduces enhanced structural imperfections due to mismatch in bond length, bond angle, etc, wherein atomic H induced optimization of growth in ICP-CVD introduces significant control of nanocrystallization in nc-Si/a-SiC heterostructure, thereby producing an efficient wide optical gap material possessing high crystallinity, suitable for applications in nc-Si solar cells and other optoelectronic devices.

Although the dissociation energy of the methane molecules (~413.0 kJ mol^{-1}) is much larger than that of the silane molecules (~299.2 kJ mol^{-1}),[55] it is expected that the RF power applied to the plasma for the present set of samples is sufficiently high to dissociate all the CH_4 and SiH_4 molecules used in limited flow rates. However, the carbon based radicals have a much lower sticking coefficient compared to the silicon-based radicals.[43,56] These two factors act in accord and eventually lead to the lower growth rates of the films at higher R, the CH_4-dilution to the SiH_4-plasma.[53] In addition, the reduced fraction of SiH_n radicals in the plasma at higher R encounters with rather higher number of atomic H decomposed from increased total flow of feedstock (SiH_4 + CH_4), which further influences in reducing the growth rate of the material due to increased atomic H etching. Accordingly, the growth parameters favour consequent lowering in the incubation layer and the surface over layer thickness at increased R, mainly by atomic H induced elimination of voids, as evidenced by the ellipsometric simulations.

The nature of variation of the carbon content in the films estimated from the C 1s XPS spectra and the composition of the amorphous component in the network estimated from ellipsometric modelling shows an excellent agreement on changes in R. The carbon content in the nc-Si/a-SiC hetero-structure increases almost linearly, attaining ~18 at.% at R=7.5 for which the amorphous component in the bulk of the material increases almost linearly from 7 to 21%. Beyond R=7.5, a very rapid incorporation of C takes place and the material contains ~44 at.% of C at R=10, while the network changes drastically towards an amorphous dominated structure having 65% of amorphous component. As no trace of c-SiC structure was identified in the network, it is reasonable to consider that carbon is preferentially incorporated in the a-Si component of the basic nc-Si/a-Si network and increasing a-SiC component induces miniaturization of Si nanocrystallites by terminating their growth. Simultaneously, increased atomic H density in the plasma containing reduced number of SiH_n precursors at higher R, as discussed above, generates larger number of c-Si nucleation centers which subsequently produces higher density of reduced size Si-ncs in the nc-Si/a-SiC heterostructure at an elevated CH_4-dilution to the SiH_4 plasma, as evidenced in Fig. 7(c). Continuous replacement of the weaker Si-Si bonds in the network by stronger Si-C bonds gradually enhances the optical band gap of the a-SiC component, as estimated by TL fitting to the ellipsometry data. Increasing C-content on the network is contributed by both Si-C and C-C components between which the intensity of Si-C relative to Si-Si increases linearly while the intensity of C-C relative to C-Si remains virtually unchanged, thereby introducing a linear increase in the total C-content in the nc-Si/a-SiC hetero-structure for $1 \leq R \leq 7.5$. Conversely, for $R > 7.5$ the Si-C bond density increases very rapidly along with a subsequent sharp increase in C-C to C-Si bond ratio, which altogether introduces a very sharp increase in the total C-content in the nc-Si/a-SiC heterostructure. However, sharp increase in C-C to C-Si bond ratio, for $R > 7.5$, introduces a notable transition in the mode of C incorporation in the Si-network. Eventually a fraction of incorporated C bonds with Si forming Si-C bonds, while the remaining part bonds with C itself, making C-C bonds which occurs at very high CH_4 dilution, at $R > 7.5$. The growth of silicon-rich Si-C films does not exclude the possibility of carbon segregation forming C-C bonds in the amorphous configuration. Formation of C-C bonds in abundance, deteriorate the Si continuous bonding network and consequently persuade formation of an amorphous dominated silicon-carbon hetero-structure containing very high density (~10^{13} cm^{-2}) of tiny (~3 nm) Si-nanocrystallites.

Conclusions

In quest of a suitable window layer for the nc-Si *p-i-n* solar cells in superstrate configuration, *p*-type nc-Si/a-SiC composite layer has been identified as the most promising one, as its a-SiC component could provide a wide optical band gap and the electrically conducting nc-Si component may assist in attaining proper crystallization of the *i*-nc-Si absorber-layer during its subsequent growth. In this regard, a systematic analysis has been performed by spectroscopic simulations and optimization on the structural composition of nc-Si/a-SiC films, prepared by varying CH_4-to-SiH_4 flow ratio (R) in the H_2-diluted SiH_4 plasma in planar inductively coupled plasma CVD. On systematic limited increase of R in the plasma, C is basically incorporated at the amorphous component of the network in the form of Si-C bonds and increases its optical band gap; simultaneously the nc-Si component reduces in volume fraction. Crystallinity in the bulk layer reduces from 80% to only 70%, Si-nanocrystals reduces in size from ~ 10 to 5 nm with narrower size distribution and increased number density from ~1.9 x 10^{12} cm^{-2} to 6.5 x 10^{12} cm^{-2}, the void fraction goes down to ~10%, while the optical gap of the a-SiC component widens from 1.67 to 1.90 eV, corresponding to inclusion of 18 at.% of C in the network. The

Physical Chemistry Chemical Physics Accepted Manuscript

This journal is © The Royal Society of Chemistry [year]

nc-Si/a-SiC thin films with negligible incubation layer of ~20-10 Å were obtained. Altogether, a stimulated nanocrystallization in the Si network induced by limited amount of carbon incorporation leads to nc-Si/a-SiC composite material, suitable for applications in nc-Si solar cells, in particular. At larger C-incorporation, formation of C-C bonds in abundance, restrains the Si continuous bonding network and persuade growth of an amorphous dominated silicon-carbon hetero-structure containing very high density (~10^{13} cm^{-2}) of tiny (~3 nm) Si-nanocrystallites. Probable growth mechanism of the nc-Si/a-SiC heterostructures from CH_4 diluted SiH_4 plasma in chemical vapour deposition has been elucidated.

The novelty of the present work is to enable spontaneous growth of self-assembled superior quality nc-Si/a-SiC thin films, corresponding to optimized inclusion of C, and simultaneous spectroscopic simulation-based optimization of properties for utilization in devices.

Acknowledgement

The work has been done under nano-silicon projects funded by Department of Science and Technology (Nano-Mission Program) and Council of Scientific and Industrial Research, Government of India. The HR-TEM and XPS studies have been performed using facilities of DST Unit on Nano-Science at IACS.

Nano-Science Group,
Energy Research Unit,
Indian Association for the Cultivation of Science,
Jadavpur, Kolkata – 700 032, India.
** Corresponding author, E-mail: erdd@iacs.res.in (D. Das);*
Fax: +91(33)24732805

References:

1 B. Yan, G. Yue, J. M. Owens, J. Yang and S. Guha, *Appl. Phys. Lett.* 2004**, 85**, 1925–1927.
2 G. Yue, B. Yan, G. Ganguly, J. Yang, S. Guha and C. W. Teplin, *Appl. Phys. Lett.* 2006, **88**, 263507.
3 D. Kar and D. Das, *J. Mater. Chem. A* **2013,** *1*, 14744–14753.
4 Z. Hu, X. Liao, H. Diao, Y. Cai, S. Zhang, E. Fortunato and R. Martins, *J. Non-Crys. Solids* 2006**, 352**, 1900–1903.
5 T. Fujibayashi and M. Kondo, *J. Appl. Phys.* 2006**, 99**, 043703.
6 K. Adhikary and S. Ray, *J. Non-Crys. Solids* 2007**, 353**, 2289–2294.
7 Y. Huang, T. Chen, A. Gordijn, A. Dasgupta, F. Finger and R. Carius, *J. Non-Crys. Solids* 2008**, 354**, 2430–2434.
8 D. Das, M. Jana and A. K. Barua, *Sol. Energ. Mat. Sol. C.* 2000**, 63**, 285–297.
9 D. Das and A. Samanta, *Nanotechnology* 2011**, 22**, 055601.
10 B. Sain and D. Das, *Phys. Chem. Chem. Phys.* 2013**, 15**,3881–3888.
11 Y. Tawada, M. Kondo,H. Okamoto and Y. Hamakawa, *Sol. Energ. Mater.* 1982**, 6**, 299–315.
12 U. Coscia, G. Ambrosone, S. Lettieri, P. Maddalena, V. Rigato, S. Restello, E. Bobeico and M. Tucci, *Sol. Energ. Mat. Sol. C.* 2005**, 87**, 433–444.
13 U. Coscia, G. Ambrosone, S. Lettieri, P. Maddalena, P. Rava and C. Minarini, *Thin Solid Films* 2003, **427**, 284–288.
14 D. Raha and D. Das, *Appl. Surf. Sci.* 2013, **276**, 249–257.
15 G. V. Bianco, M. Losurdo, M. M. Giangregorio, P. Capezzuto and G. Bruno, *Phys. Chem. Chem. Phys.* 2014**, 16**, 3632–3639.
16 D. Das, *Thin Solid Films* 2005, **476**, 237–245.
17 D. Das, *J. Appl. Phys.* 2003**, 93**, 2528–2535.
18 I. Stenger, B. Gallas, L. Siozade, C. C. Kao, S. Chenot, S. Fisson, G. Vuye and J. Rivory, *J. Appl. Phys.* 2008**, 103**, 114303.
19 D. Das, *Solid State Commun.* 2003, **128**, 397–402.
20 A. Fontcuberta i Morral, P. Roca i Cabarrocas and C. Clerc, *Phys. Rev. B* 2004**, 69**, 125307.
21 D. K. Basa, G. Abbate, G. Ambrosone, U. Coscia and A. Marino, *J. Appl. Phys.* 2010**, 107**, 023502.
22 M. I. Alonso, I. C. Marcus, M. Garriga, A. R. Goñi, J. Jedrzejewski and I. Balberg, *Phys. Rev. B* 2010, **82**, 045302.
23 M. Losurdo, M. M. Giangregorio, P. Capezzuto, G. Bruno, M. F. Cerqueira, E. Alves and M. Stepikhova, *Appl. Phys. Lett.* 2003, **82**, 2993–2995.
24 G. E. Jellison and F. A. Modine, *Appl. Phys. Lett.* 1996**, 69**, 2137–2137.
25 A. R. Forouhi and I. Bloomer, *Phys. Rev. B* 1986**, 34**, 7018–7026.
26 A. Hadjadj, N. Pham, P. Roca i Cabarrocas, O. Jbara, and G. Djellouli, *J. Appl. Phys.* 2010**, 107**, 083509.
27 P. Petrik, M. Fried,E. Vazsonyi, P. Basa,T. Lohner, P. Kozma and Z. Makkai, *J. Appl. Phys.* 2009**, 105**, 024908.
28 M. Daouahi and N. Rekik, *J. Phys. Chem. C* 2012**, 116**, 21018–21026.
29 J. Tauc, R. Grigorovici and A. Vancu, *Phys. status solidi (b)* 1966**, 15**, 627–637.
30 H. G. Tompkins, E. A. I., *Handbook of Ellipsometry*. William Andrew: New York, 2005.
31 G. E. Jellison Jr, *Thin Solid Films* 1993**, 234**, 416–422.
32 Q. Cheng, S. Xu and K. Ostrikov, *J. Phys. Chem. C* 2009, **113**, 14759 –14764.
33 S. Guha, G. Hendershot, D. Peebles, P. Steiner, F. Kozlowski and W. Lang, *Appl. Phys. Lett.* 1994, **64**, 613–615.
34 D. Raha and D. Das, *Sol. Energ. Mat. Sol. C.* 2011, **95**, 3181–3188.
35 S. Veprek, F. A. Sarott and Z. Iqbal, *Phys. Rev. B* 1987, **36**, 3344–3350.
36 D. Das, M. Jana, A. K. Barua, S. Chattopadhaya, L. C. Chen and K. H. Chen, *Jpn. J. Appl. Phys.* 2002, **41**, L229–L232.
37 V. Paillard, P. Puech, M. A. Laguna, R. Carles, B. Kohn and F. Huisken, *J. Appl. Phys.* 1999, **86**, 1921–1924.
38 G. Faraci, S. Gibilisco, A. R. Pennisi and C. Faraci, *J. Appl. Phys.* 2011, **109**, 074311.
39 W. W. Ke, X. Feng and Y. D. Huang, *J. Appl. Phys.* 2011, **109**, 083526.
40 D. Barba, F. Martin and G. G. Ross, *Nanotechnology* 2008, **19**, 115707.
41 X. Liu, Y. Zhang, D. Ge, J. Zhao,Y. Li and F. Endres, *Phys. Chem. Chem. Phys.* 2011, **23**, 5219–5223.
42 W. K. Choi, T. Y. O., L. S. Tan, F. C. Loh, and K. L. Tan, *J. Appl. Phys.* 1998, **83**, 4968.
43 Q. Cheng, S. Xu and K. Ostrikov, *Acta Materialia* 2010, **58**, 560–569.
44 Q. Cheng, E. Tam, S. Xu and K. Ostrikov, *Nanoscale* 2010, **2**, 594–600.
45 M. Jana, D. Das, S. T. Kshirsagar and A. K. Barua, *Jpn. J. Appl. Phys.* 1999, **38**, L1087–L1090.
46 D. Das and M. Jana, *Sol. Energ. Mat. Sol. C.* 2004, **81**, 169–181.
47 D. Das, *Solid State Commun.* 1998, **108**, 983–987.
48 S. Xu, K. Ostrikov, Y. Li, E. L. Tsakadze and I. R. Jones, *Phys. Plasmas* 2001, **8**, 2549–2557.
49 J. H. Zhou, K. Ikuta, T.. Yasuda, T. Umeda, S. Yamasaki and K. Tanaka, *Appl. Phys. Lett.* 1997, **71**, 1534–1536.
50 S. Y. Myong, S. S. Kim and K. S. Lim, *J. Appl. Phys.* 2004, **95**, 1525–1530.
51 T. Chen, Y. Huang, A. Dasgupta, M .Luysberg, L. Houbenc, D. Yang, R. Carius and F. Finger, *Sol. Energ. Mat. Sol. C.* 2012**, 98**, 370–378.
52 C. Song, Y. Rui, Q. Wang, J. Xu, W. Li, K. Chen, Y. Zuo and Q. Wang, *J. Alloy. Compd.* 2011**, 509**, 3963–3966.
53 J. Robertson, *Philos. Mag. B* 1992**, 66**, 615–638.
54 D. Das, *Solid State Phenom.* 1995, **44**, 227–260.
55 Q. Cheng, S. Xu, J. D. Long, Z. H. Ni, A. E. Rider and K. Ostrikov, *J. Phys. D: Appl. Phys.* 2008, **41**, 055406.
56 C. C. Liu, C. Lee, K. L. Cheng, H. C. Cheng and T. R. Yew, *Appl. Phys. Lett.* 1995, **66**, 168–170.

Physical Chemistry Chemical Physics Accepted Manuscript